High resolution description of a crack front in a heterogeneous Plexiglas block

Arnaud Delaplace,[1,2] Jean Schmittbuhl,[3] and Knut Jørgen Måløy[1]
[1]*Fysisk Institutt, Universitetet i Oslo, P.O. Boks 1048 Blindern, 0316 Oslo 3, Norway*
[2]*Laboratoire de Mécanique et Technologie, Ecole Normale Supérieure de Cachan, Avenue du Président Wilson, F-9 Cachan, France*
[3]*Laboratoire de Géologie, Ecole Normale Supérieure, 24 rue Lhomond, 75231 Paris Cedex 05, France*
(Received 10 March 1999)

We study experimentally the propagation of an in-plane fracture into a transparent and heterogeneous Plexiglas block. A stable crack propagation in mode I is monitored by an imposed displacement. The experimental setup allows a high resolution observation of the crack front *in situ*. Self-affine properties of the crack front are described over more than three decades using several techniques: variable bandwidth, return probability, Fourier spectrum, and wavelet analysis. The different methods lead to a roughness exponent of 0.63 ± 0.03, consistent with a previous work. [S1063-651X(99)01608-6]

PACS number(s): 62.20.Mk, 46.50.+a, 61.43.−j, 81.40.Np

I. INTRODUCTION

As first mentioned in the early work by Mandelbrot, Passoja, and Paullay [2], fracture surfaces exhibit scaling invariances. In recent years many experiments have shown the self-affinity of crack surfaces [3–9], with a roughness exponent close to 0.8 for the three-dimensional crack surface. This roughness exponent is found to be very robust for many different materials and different fracture modes [4]. A possible universal roughness exponent was first conjectured in Ref. [4]. Experimentally it is very difficult to verify this universality owing to the limited number of measurements and the uncertainties of the experimental estimates that are often larger than observed fluctuations. From a theoretical point of view, self-affine properties of crack fronts and the universality of the roughness exponent are challenging questions. The physical origin of the very long range correlations along the crack front is not fully understood.

The front line of a fracture propagating in a three-dimensional medium has a three-dimensional shape with both in-plane and out-of-plane roughnesses. The morphology of this fracture front controls the morphology of the final fracture surface at any time. More precisely, the out-of-plane roughness monitors the roughness of the crack surface. However, in-plane and out-of-plane roughnesses of the crack are linked [10], and the long-range correlations along the in-plane fracture front may explain the correlations within the fracture surface. It was suggested by Bouchaud *et al.* [10] that the work by Ertas and Kardar [11] might be applicable to fractures. They used local interactions and an annealed noise. Ramanathan *et al.* [12] studied the case of nonlocal elastic interactions in the quasistatic limit. A second approach has been initiated from the work of Rice and co-workers [13,14], and limits the analysis to planar cracks [15–17]. The driving force is the stress intensity factor which includes a nonlocal kernel resulting from the bulk elasticity of the medium. This model was used with an external dynamics introducing spatial fluctuations of the toughness as a quenched noise [15]. In the quasistatic regime, the front is self-affine with a roughness exponent of 0.35. More recently Fisher and co-workers [17,18] obtained similar results either numerically or analytically using the renormalization group theory.

The study of the fracture front line has received little attention by experimentalists because of the difficulty of making direct observations of the crack front. The authors of Ref. [19] cast a crack tip by stopping the crack propagation and injecting ink into the fracture under a moderate vacuum. After having dried the sample and completed the fracture, the fracture front was extracted from the front between covered and non-ink-covered metal. The self-affine exponent describing the in-plane roughness of the crack was found to be $\zeta = 0.60$. Mower and Argon [20] directly measured the propagation of a crack in a transparent epoxy. However, in this case, defaults were not randomly distributed.

In this work we present an experimental setup that allows a direct observation of an in-plane crack front which propagates into the annealing plane of two polymethylmethacrylate (PMMA) blocks. The important features of our setup are the transparency the PMMA and the random toughness introduced along the weak plane by a sand-blasting procedure. Furthermore we are able to obtain a high dynamic resolution of the front by linking together several pictures. The roughness analysis is subsequently made on a large range of length scales which significantly increases the measure reliability. Most previous measurements have been made after the final propagation of the crack. In this work wide fracture fronts are observed at different positions during a quasistatic crack propagation within the same sample. We checked carefully for most experimental drawbacks, and analyzed the roughness of the crack front using several independent techniques. Experimental estimates of the crack front roughness exponent obtained in this work confirm results obtained in a preliminary work [1].

In Sec. II of this paper, we give a full description of the sample preparation and of the mechanical and the optical setups. Section III presents image processing and data analysis. Finally, the estimates of the roughness exponent obtained from different methods are discussed, and compared with previous works.

II. EXPERIMENTAL SETUP

A. Sample preparation

The aim of this work is to observe and characterize an in-plane crack front during its propagation in a heteroge-

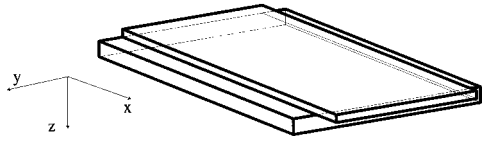

FIG. 1. The Plexiglas sample is built from two PMMA plates: a thick one that is 32 cm long, 14 cm wide, and 1 cm thick, and a thin one that is 34 cm long, 12 cm wide, and 0.4 cm thick. Both plates are joined by a sintering process.

neous medium. Samples are made of polymethylmethacrylate GS (PMMA) which is transparent. Each sample is built using two PMMA plates: a thick one which is 32 cm long, 14 cm wide, and 1 cm thick and a thin one that is 34 cm long, 12 cm wide, and 0.4 cm thick. The plates are annealed together by increasing temperature and pressure. A normal homogeneous pressure is applied on both sides of the sample using a press made of two parallel aluminum plates and loaded with eight clamps. The temperature is controlled in a precisely regulated ceramic oven at 205 °C for 30 min. A slow ramp is imposed either to heat or cool the sample to avoid thermal stresses. Finally we obtain one block with a weak annealing plane where the crack will propagate (see Fig. 1). The crack plane is referred as (x,y): the x axis is along the crack propagation direction, and the y axis is parallel to the mean crack front. The z axis is normal to this plane.

Each plate is sand blasted on the side to be annealed. Surfaces are blown with a air jet to remove dust after sand blasting. One important consequence of the sand blasting is that the transparency of the PMMA is lost. Light scatters from introduced microstructures along sand-blasted surfaces. However, after the annealing procedure the newly formed block recovers its transparency. New polymer chains are formed through the rough interface, and air bubbles are extracted with the pressure load. Differences of the refraction indexes along the interfaces disappears. Conversely, when both plates are moved apart during the fracture propagation, the polymer chains are broken and air is introduced. Differences of refraction indexes across the interface are recovered and the fractured surface appears as opaque. The transition between the transparent and the opaque areas corresponds to the crack front.

The sand-blasting procedure also introduces a random uncorrelated roughness on the surfaces. The magnitude of the roughness is less than a few micrometers. Using a microscope we checked the random position of the default and the maximum size of the default: about 50 μm corresponding to the bead size of the sand. This length scale is much smaller than the largest scale observed in this experiment which is of the order of several mm. The height fluctuations introduced by the sand-blasting procedure introduce fluctuations of the toughness along the interface. We expect the toughness to be spatially uncorrelated, at least on length scales larger than the bead size. However, the exact relationship between the roughness and the toughness fluctuations is extremely difficult to quantify experimentally and is an open question.

The annealing process (specially its uniformity) was checked by visual inspection with a microscope. In order to check that the plates were sufficiently annealed, a colored nigrosine water solution was injected within the fracture at a given position of the crack front. It is important to note that the water wets the Plexiglas and spontaneously invades any free open space between the plates. No transport of water nigrosine solution was observed across the fracture front, indicating a continuous soldering of the plates without air bubbles trapped in the annealed part.

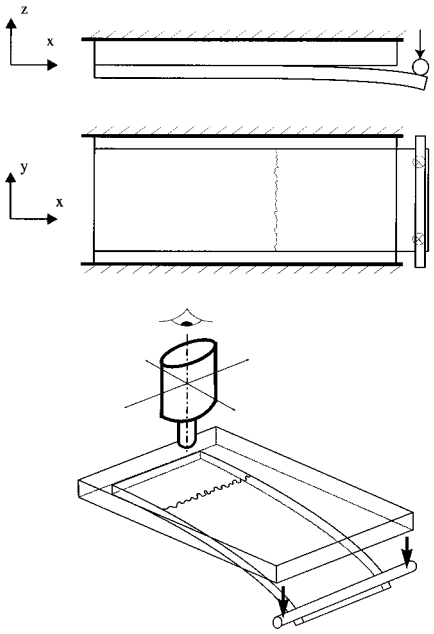

FIG. 2. Scheme of the mechanical setup: the thick plate is clamped into a rigid frame. The displacement is imposed on the thin plate with cylindrical rod.

B. Mechanical setup

The thick plate of the PMMA block is clamped to a stiff aluminum frame. A normal displacement is imposed to the thin plate with a rod (see Fig. 2), which induces a stable crack propagation in mode I. Oil is added on the contact between the rod and the plate to reduce friction and subsequently shear loading of the fracture. The rod is moved vertically quasistatically using a stepping motor. The imposed displacement rate is typically of the order of 10^{-7} m/s. However, the loading is stopped regularly to arrest the front propagation and take pictures of the crack front. This stopping procedure should not influence the crack front roughness, since it was shown [1] using the same setup that the roughness exponent is independent of the crack speed for low speeds (from 10^{-7} to 5×10^{-5} m/s).

C. Optical setup

The crack front is observed with a microscope linked to a Kodak DCS 420 CCD camera which has a resolution of 1536×1024 pixels. The visualization setup is mounted on a translation table that moves parallel to the propagation plane (x,y). The table is controlled by two stepping motors with a precision of 3.125 μm in both directions x and y.

During each loading stop, the table is translated along the front (y axis), and neighboring pictures were taken. The assemblage of up to 20 pictures provides a large front description of 2^{14} $(=16\,384)$ data points. Each picture shows 4 mm of the front along the y direction. Two neighboring pictures

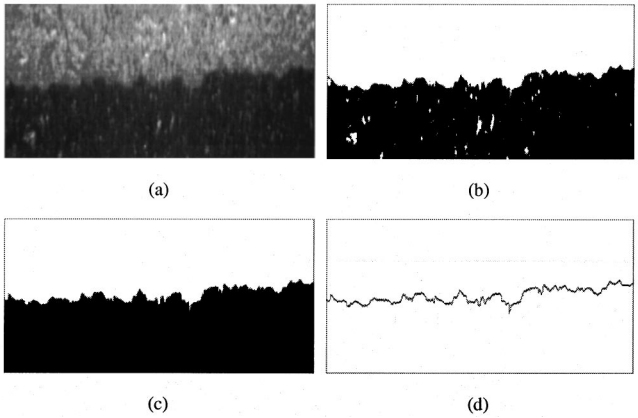

FIG. 3. Image treatment of a crack front picture. (a) shows the raw picture. (b) is after threshold. (c) shows the picture after the cluster extraction and (d) the extracted front. Note that a vertical scaling ratio of 4 is applied to all the pictures in order to magnify the roughness.

are taken with an overlap of one-third of the picture width. The total length of the analyzed crack is subsequently around 50 mm. The roughness of the front along the x direction is less than 0.3 mm.

In order to have a sufficient, homogeneous, and constant contrast between the opaque and transparent zones, the crack front is illuminated with a lamp that moves with the visualization setup. The light beam is perpendicular to the crack front, and is wide with respect to the picture width.

III. CRACK FRONT OBSERVATION

The front path is extracted from a front picture [see Fig. 3(a)] using an image treatment procedure. First we compute the histogram of the gray levels of the picture (Fig. 4). This histogram shows clearly two peaks which correspond, respectively, to the soldered part (dark gray) and the unstuck one (bright gray). By thresholding the images at a level that separates both peaks [Fig. 3(b)], the soldered part becomes black, and the unstuck one becomes white. The next step is to remove all small clusters, i.e., the white pixels in the black part, and the black pixels in the white part [Fig. 3(c)]. Finally we extract the front path by computing the gradient of the pixel levels. This provides the boundary between the white and the black parts [Fig. 3(d)], which is the crack front.

As mentioned above, pictures are obtained from a microscope and a CCD camera. These two pieces of equipment induce a deformation of the real image because of the lenses. In order to quantify this effect, a calibration test has been performed taking pictures of the boundary of a razor blade. We found that the deformation along the crack propagation (the x axis) was very small and could be neglected. Conversely, a significant deformation was observed along the y direction. This deformation transformed a line into a parabola which depends on the line position in the picture. We moved the blade from the bottom to the top of the picture (parallel to the y axis) using many steps. For each step the deformation (i.e., the parabola) was measured, providing a map of the lens deformation. This mapping was used to correct for the lens deformations of the crack fronts.

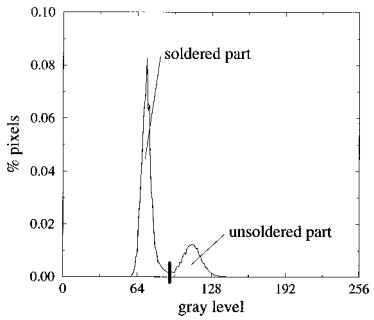

FIG. 4. A sample of the gray histogram of one front image. The scale extends from 0 (black) to 255 (white). The chosen threshold is shown as a black vertical line.

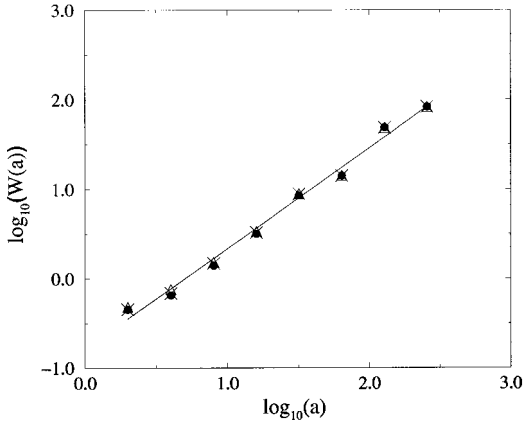

FIG. 5. Wavelet analysis with three fronts obtained from the same picture but with three different thresholds [92 (●), 93 (×), and 94 (△) on the 0–256 gray level]. The slope of the best fitted line is weakly affected affected (2%).

The front description depends strongly on the thresholding procedure. Although the gray level histogram shows two well separated peaks relative to the soldered and unstuck parts, an overlap of the peaks exists. In order to evaluate the influence of this overlap, several fronts have been extracted from the same picture but using different thresholds chosen within the vicinity of the minimum between the two gray level peaks (Fig. 4). From Fig. 5, we see that a small variation of the threshold (± 1 gray level) does not significantly affect the estimates of the roughness exponent (using wavelet analysis) ± 0.02, and can be neglected.

A complete description of the front shows local overhangs [see Fig. 6(a)]. However, roughness analysis methods require single valued functions [sets of pairs (x_i, y_i), with $x_i < x_{i+1}$] of the front path. Two different ways were chosen to obtain single valued functions: either the upper points [Fig.

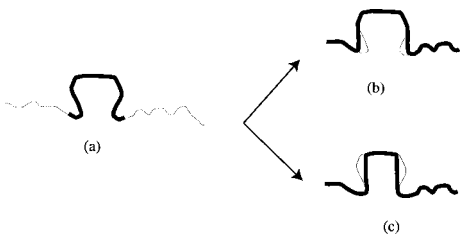

FIG. 6. Overhangs along the crack front (a). The crack front path is obtained from the upper points (b) or the lower points (c).

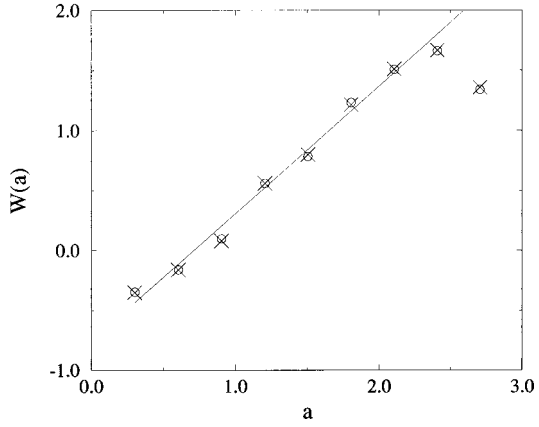

FIG. 7. Two wavelet analyses of the same front using either the upper points (○) or *lower* points (×) to describe the crack front path.

6(b)], or the lower points are kept [Fig. 6(c)]. As seen in Fig. 7, the roughness exponent (using wavelet technique) is not sensitive to these changes. This result is confirmed by the small number of the overhangs: their size is characterized by the number of multiple valued abscissas. An analysis of seven pictures gives on average a frequency of multiple valued abscissas lower than 3%. Arbitrarily, we chose the procedure using the lower points for our analysis.

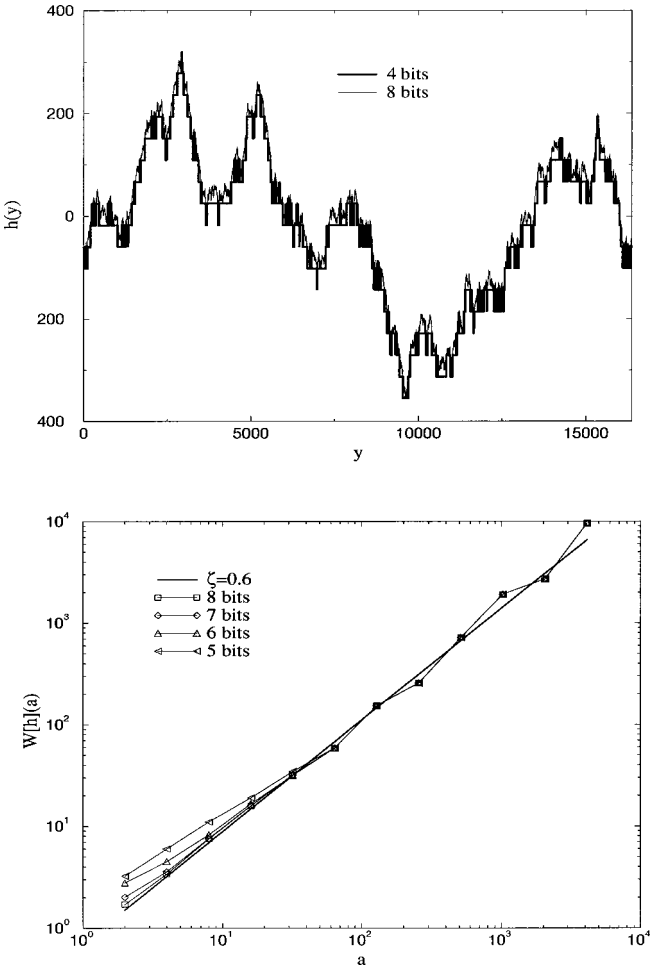

FIG. 8. The upper figure shows the same synthetic profile using two different resolutions: four bits and eight bits for the local height definition. The lower picture shows the scaling using the average wavelet coefficient method applied to the same front filtered at different resolutions: five, six, seven, or eight bits.

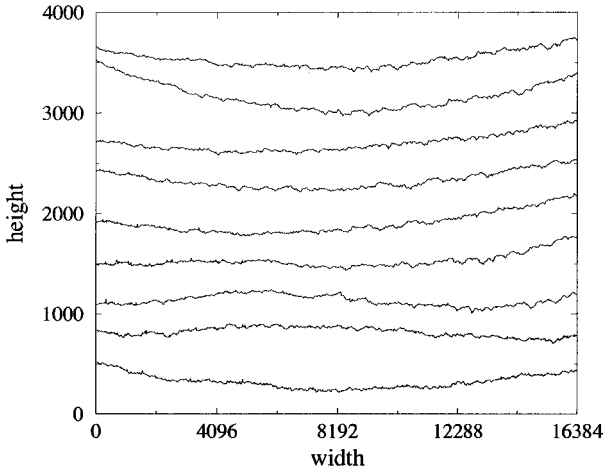

FIG. 9. Nine fronts obtained for a quasistatic propagation. Each front description is obtained by linking 20 pictures taken during a stop of the loading and a sweep over the crack front. Fronts obtained at different time steps are superimposed on the same figure.

The precision of the translation table is checked by taking two pictures of the same front before and after a back and forth move of the table. After a subtraction of the pictures, we never observed a translation larger than two pixels, which is small with respect to the total magnitude of front roughness (larger than 100 pixels).

We also checked the influence of the discrete description of the crack front path. The total magnitude of the roughness corresponds to 100 pixels. Roughness fluctuations are sampled with a limited number of levels. We verified that this limited resolution was not influencing the roughness analysis. We built synthetic self-affine profiles with the observed roughness exponent and filtered them using different resolutions: five bits, six bits, seven bits, and eight bits. The scaling properties of the front is analyzed with the average wavelet coefficient method (Fig. 8). We observe that the resolution affects the scaling for small scales. However for resolution larger than seven bits (i.e., 128 height levels) the scaling estimate is very weakly altered, and confirms the sufficient precision of the experimental setup.

IV. SCALING ANALYSIS OF THE CRACK FRONT

The roughness exponent is computed from four independent techniques: the variable bandwidth method, the return method, the power spectrum analysis (see, for instance, Ref. [21] for a description of these techniques), and the average wavelet coefficient (AWC) method [22]. Nine independent fronts of 16 384 points have been extracted from two PMMA samples, and analyzed (Fig. 9). This is a much larger data set compared to previous works (see Refs. [9,19], and references therein), and provides a large scaling range for measurement of the roughness exponent.

The variable bandwidth method swept over profiles windows of different sizes. A window of size Δ is moved along the profile and the standard deviation ω of the height within the window is averaged over all the window position x_0. The

TABLE I. Estimates of the roughness exponent of the crack front using four independent techniques: the variable bandwidth method, the multireturn method, the Fourier spectrum, and the average wavelet method (see the text for a full description).

	Bandwidth method	Multiple return method	Power spectrum analysis	AWC method
front1	0.66	0.48	0.65	0.65
front2	0.60	0.46	0.54	0.60
front3	0.60	0.53	0.60	0.62
front4	0.65	0.51	0.63	0.65
front5	0.57	0.54	0.58	0.63
front6	0.65	0.58	0.67	0.63
front7	0.70	0.49	0.74	0.66
front8	0.66	0.60	0.71	0.71
front9	0.63	0.52	0.62	0.61
mean (rms)	0.64 ± 0.04	0.52 ± 0.04	0.64 ± 0.06	0.64 ± 0.03
fit	0.63 ± 0.03	0.55 ± 0.05	0.64 ± 0.03	0.63 ± 0.03

roughness exponent ζ is obtained from the relation [23] $(\omega)_{x_0}\propto\Delta^{\zeta}$.

Here we also consider the multireturn probability with a logarithmic binning. In this method the profile is cut from its minimum to its maximum by a horizontal line. For each line all distances d which separate two intersection points (between the line and the profile) are computed. The histogram p_m of the distances d verifies the relation: $p_m(d)\propto d^{1-\zeta}$ in case of self-affinity [7].

The power spectrum analysis is based on the computation of the power spectrum $S(f)$. For a self-affine profile the roughness exponent follows [24] $S(f)\propto f^{1-2\zeta}$.

An average wavelet coefficient method was proposed in Ref. [22]. It is based on the computation of the wavelet transform of a function h using Daubechies wavelet filters with 12 coefficients. For a self-affine function, it can be shown that the average of wavelet coefficients over the translation factor b verifies $W[h](a)\propto a^{(1/2)+\zeta}$, where a is the spatial scale parameter of the wavelet.

Results of the self-affine analyses are summarized in Table I. For each front, the roughness exponent is measured using four different methods. The two last lines correspond to different averages for all methods. The first value is the average of the exponent estimates obtained for each of the nine fronts. The error bar results from the rms of all the nine values. The last value is found by a linear fitting of curves (Figs. 10–13) obtained by averaging the analysis curves of each of the nine fronts. The error bar in this case is an estimate of error during the fitting procedure. Both averaging procedures lead to very similar results. Finally, we propose the estimate of the roughness exponent to be $\zeta=0.63\pm0.03$, which is a mean of the different values, excepted of the multiple return method value. This choice is justified by the large gap between this value and the others. Furthermore, the power spectrum analysis and the AWC method are known to be the more reliable methods [21,22]. The result is consistent within the error bars with our previous work [1].

V. CONCLUSION

An extensive roughness analysis of an in-plane fracture front propagating in a Plexiglas block with a heterogeneous toughness have been performed. We obtained a high resolu-

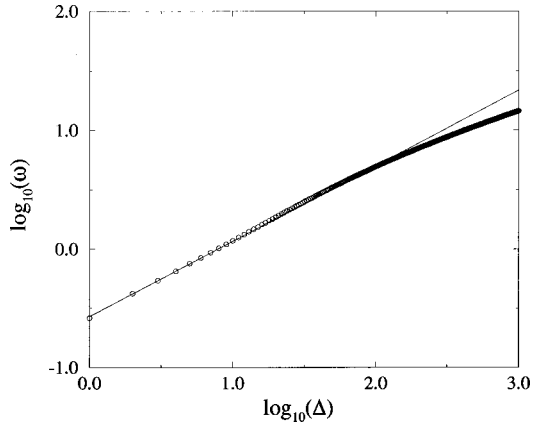

FIG. 10. Average of the variable bandwidth analysis over the nine fronts in a log-log diagram. The best fitted line has a slope of $0.63=\zeta$, where ζ is a roughness exponent.

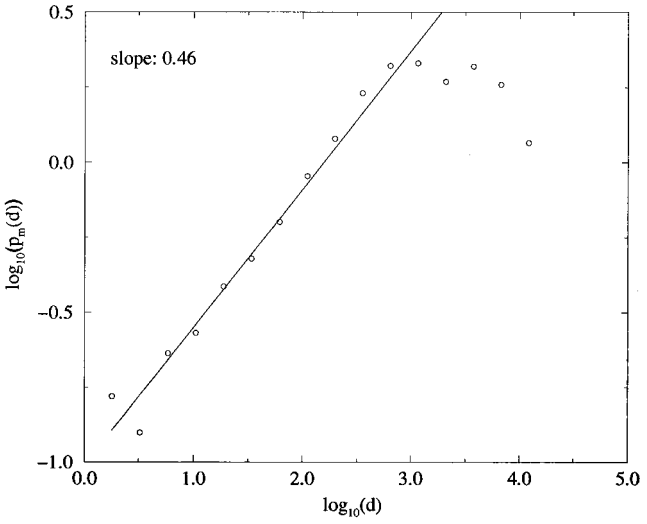

FIG. 11. Average of the multiple return probability analysis over the nine fronts in a log-log diagram. The best fitted line has a slope of $0.46=1-\zeta$, where ζ is a roughness exponent.

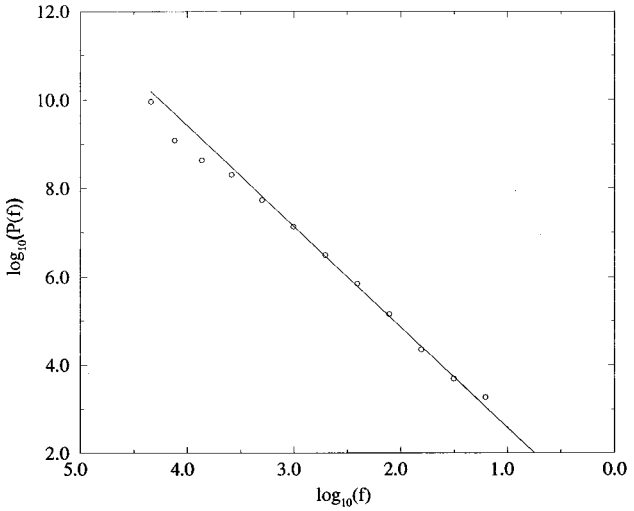

FIG. 12. Average of the power spectrum analysis over the nine fronts in a log-log diagram. The best fitted line has a slope of $2.28=1-2\zeta$, where ζ is a roughness exponent.

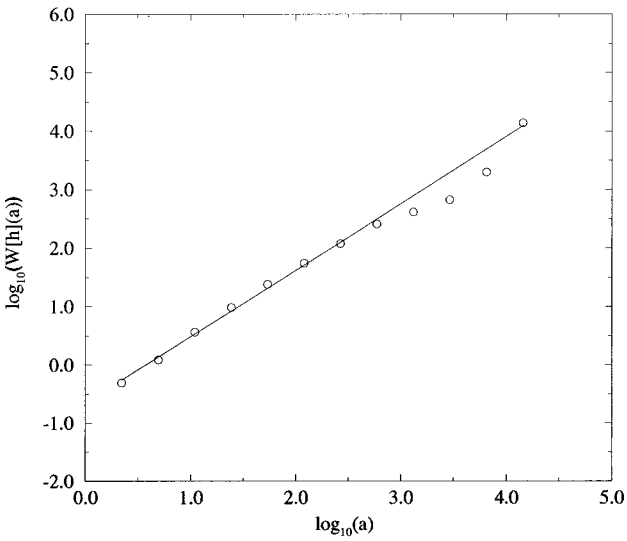

FIG. 13. Average of the wavelet analysis of the nine fronts in a log-log diagram. The best fitted line has a slope of $1.13=1/2+\zeta$, where ζ is a roughness exponent.

tion description of the front which provides a significant increase in the dynamic range of length scales compared to previous work [1], and makes possible a reliable estimate of the roughness exponent. Large fronts were obtained by using a translational microscope along the crack front at rest. The link of 20 different pictures gives a discrete representation of 2^{14} points per front position. The picture link requires to filter the image deformation resulting from the camera and microscope lenses.

The roughness exponent has been analyzed by using four different techniques. By averaging the results from the different techniques we found a roughness exponent $\zeta=0.63\pm0.03$. This result is consistent with previous measurements [1] ($\zeta=0.55\pm0.05$) on much smaller fronts.

The roughness exponent obtained is not consistent with any existing theoretical models [15,25,26,10]. However, these models do not contain any long range correlations in the noise. It is not clear at the moment if there are correlations in the toughness introduced by the sand-blasting procedure. However since the correlations in height fluctuations introduced by the sand-blasting procedure have a cutoff length around 50 μm, we expect the toughness to be uncorrelated on a length scale larger than this length. The influence of spatially correlated roughness was explored recently by Schmittbuhl and Vilotte [27]. It was shown that the roughness exponent of the crack front might be significantly increased by any spatial correlations of the toughness. Ramanathan, Ertas, and Fisher suggested that the fracture load mode may influence the spatial correlations along the crack front [12]. The viscous-elastic properties of the plexiglas might involve a large range of time scales which may give rise to effective spatial correlations in the system.

One important feature of the present experimental system is that it is well suited for *in situ* dynamic studies of fracture propagation due to the movable microscope. This work is in progress.

ACKNOWLEDGMENTS

We acknowledge J. P. Vilotte and S. Roux for helpful comments and useful discussions. This work was supported by the CNRS and NFR through a ''Programme International de Coopération Scientifique'' grant.

[1] J. Schmittbuhl and K. Måløy, Phys. Rev. Lett. **78**, 3888 (1997).
[2] B. B. Mandelbrot, D. E. Passoja, and A. J. Paullay, Nature (London) **308**, 721 (1984).
[3] S. R. Brown and C. H. Scholz, J. Geophys. Res. **90**, 12575 (1985).
[4] E. Bouchaud, G. Lapasset, and J. Planès, Europhys. Lett. **13**, 73 (1990).
[5] J. Schmittbuhl, S. Gentier, and S. Roux, Geophys. Res. Lett. **20**, 639 (1993).
[6] B. L. Cox and J. S. Y. Wang, Fractals **1**, 87 (1993).
[7] K. J. Måløy, A. Hansen, E. L. Hinrichsen, and S. Roux, Phys. Rev. Lett. **68**, 213 (1992).
[8] J. Schmittbuhl, F. Schmitt, and C. H. Scholz, J. Geophys. Res. **100**, 5953 (1995).
[9] E. Bouchaud, J. Phys.: Condens. Matter **9**, 4319 (1997).
[10] J. P. Bouchaud, E. Bouchaud, G. Lapasset, and J. Planès, Phys. Rev. Lett. **71**, 2240 (1993).
[11] D. Ertaş and M. Kardar, Phys. Rev. Lett. **69**, 929 (1992).
[12] S. Ramanathan, D. Ertas, and D. S. Fisher, Phys. Rev. Lett. **79**, 873 (1997).
[13] J. R. Rice, J. Appl. Mech. **52**, 571 (1985).
[14] H. Gao and J. R. Rice, ASME J. Appl. Mech. **56**, 828 (1989).
[15] J. Schmittbuhl, S. Roux, J. P. Vilotte, and K. J. Måløy, Phys. Rev. Lett. **74**, 1787 (1995).
[16] P. Thomas and M. Paczuski, e-print, cond-mat/9602023.
[17] S. Ramanathan and D. Fisher, Phys. Rev. Lett. **79**, 877 (1997).
[18] D. Fisher, Phys. Rep. **301**, 113 (1998).
[19] P. Daguier, E. Bouchaud, and G. Lapasset, Europhys. Lett. **30**, 367 (1995).

[20] T. M. Mower and A. Argon, Mech. Mater. **19**, 343 (1995).
[21] J. Schmittbuhl, J. P. Vilotte, and S. Roux, Phys. Rev. E **51**, 131 (1995).
[22] I. Simonsen, A. Hansen, and O. Magnar Nes, Phys. Rev. E **58**, 2779 (1998).
[23] J. Feder, *Fractals* (Plenum, New York, 1988).
[24] K. J. Falconer, *Fractal Geometry: Mathematical Foundations and Applications* (Wiley, New York, 1990).
[25] S. Ramanathan and D. Fisher, Phys. Rev. B **58**, 6026 (1998).
[26] S. Roux and A. Hansen, J. Phys. I **4**, 515 (1994).
[27] J. Schmittbuhl and J. P. Vilotte, Physica A (to be published).